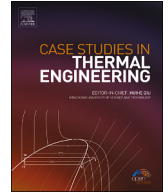


Contents lists available at [ScienceDirect](https://www.sciencedirect.com)

Case Studies in Thermal Engineering

journal homepage: www.elsevier.com/locate/csite

Thermo-fluidic behavior and entropy interpretation of ternary hybrid nanofluid inside an inclined domain having semi-circular heater and triangle-shaped corrugated walls

M.K. Nayak^{a,*}, Mohammed K. Al Mesfer^b, Amjad Ali Pasha^c, Mohd Danish^b, Kashif Irshad^d, Ali J. Chamkha^e

^a Department of Mechanical Engineering, ITER, Siksha 'O' Anusandhan Deemed to be University, Bhubaneswar, 751030, India

^b Chemical Engineering Department, College of Engineering, King Khalid University, Abha, Saudi Arabia

^c Aerospace Engineering Department, King Abdulaziz University, Jeddah, 21589, Saudi Arabia

^d Interdisciplinary Research Centre for Sustainable Energy Systems (IRC-SES), Research Institute, King Fahd University of Petroleum and Minerals (KFUPM), Dhahran, 31261, Saudi Arabia

^e Faculty of Engineering, Kuwait College of Science and Technology, Doha District, Kuwait

ARTICLE INFO

Keywords:

Ternary hybrid nanofluid
Natural convection
Heat generation/absorption
Entropy

ABSTRACT

The present work deals with thermal aspect and entropy of ternary hybrid nanofluid (Graphene, Al_2O_3 , and MWCNT as nanoparticles and water as base fluid) inside an inclined domain considering heat generation/absorption. The domain possesses triangle-shaped corrugated walls with variable height and a semi-circular heater located on its bottom wall. Finite element method (FEM) is employed to acquire a well-defined solution of the non-dimensional governing equations along with the boundary conditions. The influence of the pertinent parameters along with their ranges ($0.2 \leq b \leq 0.3$), ($10^5 \leq Ra \leq 10^6$), ($0^\circ \leq \eta \leq 90^\circ$), ($-1 \leq Hs \leq 1$) has been studied. Some striking outcomes of the present investigation are that streamlines and entropy generation (En_T) peter out while local Nusselt number (Nu_{loc}) and average Bejan number (Be_{ave}) ameliorate with rise in dimensionless height of the corrugated wall (b). The absolute maximum values of vertical and horizontal velocities of ternary hybrid nanofluid enhance by 96.47 % and 29.5 %, respectively, when inclination angle (η) increases from 45° to 90° . It is visualized that Nusselt number is maximum subject to heat sink while it attains a minimum value in response to heat source. Because of triangle shaped corrugated walls and ternary hybrid nanofluid, the present problem contributes superior cooling in thermal systems featured with such complex geometry in industries.

1. Introduction

Ternary hybrid nanofluids (THNFs) are developed by dispersing three different kinds of nanomaterials into the base fluid [1]. THNFs motivated engineers and scientists due to their distinct molecular structure and enhanced heat transfer (HT) capabilities (better thermal conductivity) [2]. Enriched with such distinguished characteristics, THNFs contribute considerable cooling in aerodynamics, solar collectors, natural convection enclosures, biomedical and chemical engineering, aerospace technology, transportation, and electronic industries. Recently the investigations of the boundary layer flow of THNFs and thermal aspects associated with them

* Corresponding author.

E-mail address: mkn2122@gmail.com (M.K. Nayak).

<https://doi.org/10.1016/j.csite.2024.104434>

Received 21 January 2024; Received in revised form 19 April 2024; Accepted 20 April 2024

Available online 23 April 2024

2214-157X/© 2024 The Authors. Published by Elsevier Ltd. This is an open access article under the CC BY-NC-ND license (<http://creativecommons.org/licenses/by-nc-nd/4.0/>).

are promising and enlightening in order to satisfy the industrial demands of better and vast cooling [3]. Many researchers carried out investigations regarding the flow and thermal behavior of different THNFs subject to surfaces of different geometries under the impact of various constraints of motion. For instance, Wenhao et al. [4] studied the dynamics of THNF at diverse levels of partial slip. They found in their study that the lowest reducing rate of the friction becomes apparent at greater levels of buoyant forces in the case of the transport phenomena being induced via free convection. Due to the escalating random movement of the three types of nanomaterials in the THNF, optimal increasing mass/species transfer rates are made possible. Using blend of distilled water and ethylene glycol, Zahan and Khatun [5] perused thermal proficiency of THNFs using a convergent-divergent nozzle. All base liquid mixes with the nanoparticle ratio (1/6:2/3:1/6) exhibit a comparatively higher heat transfer rate than other combinations. Laminate shape nanoparticles are also used to find a high rate of heat transmission. Using GFEM, Abbasi and Ashraf [6] investigated the heat transfer behaviour of THNF in radiated channel under various physical conditions. They found that the THNF is a better heat-transfer fluid than the typical binary nanofluid. Additionally, convection through the plate and induction of solar thermal radiations are crucial sources to increase the internal heat transfer of THNF and would enable researchers and engineers to develop large-scale usages. The dynamics of THNFs resulting from dual stretching on wedge planes with small and high volume fractions were examined by Xiu et al. [7]. In a parabolic trough solar collector, HT simulation of THNF flow between parallel planes was analyzed by Rawat et al. [8] utilizing particle swarm optimization and artificial neural network. Mohanty et al. [9] scrutinized the thermal performance and irreversibility of non-linear radiative cross-THNF flow around a stretched cylinder. It was discovered that an increase in curvature and Weissenberg parameters quickens the flow of fluid and the pace at which heat is transferred, while magnetic field strength can control fluid motion. Sarangi et al. [10] investigated the hydrothermal and irreversibility behaviour of the Bödewadt flow caused by a stretched spinning disc in ternary composite nanomaterial. Kumar and Hassan [11] examined heat transmission in a flat tube automobile radiator using CuO–MgO–TiO₂ THNF. A comparative analysis of ternary hybrid (graphene/zirconium oxide/magnesium oxide) and hybrid (graphene/magnesium oxide) nanomaterials over a mobile surface was conducted by Prakasha et al. [12]. It is observed that the rate of heat transfer of THNFs improves than that of HNF. Raju et al. [13] examined the nonlinear axisymmetric flow of THNFs in an expanding or contracting porous Darcy wall.

In many industrial production processes, natural convection (NC) is highly essential. Uneven density distribution causes a flow known as natural convection, which is directly applicable to many engineering applications ([14,15]). The geometry and thermo-physical characteristics of liquids may be the two most important aspects in natural convection flows, which are particularly complex due to thermal-buoyancy consequences. The positioning and shape of the domain, the heating properties, and the product characteristics may all affect the many uses of NC ([16,17]). Additionally, numerical modelling eliminates high experimental expenditures. As a result, this phenomena is now being studied in a variety of fields, including geophysics, solar distillers, fire management, and meteorology. Numerous technical uses of natural convection in confined spaces serve modern industries ([18–20]). Wang [21] studied NC inside multi-tube horizontal cylinder subject to melting process. The findings showed that with a high Rayleigh number (Ra) value, both the melting rate and the quantity of energy stored are accelerated. Due to the buoyancy effect, the upper-half portion experiences a higher melting rate than the lower-half part. Additionally, when using many tubes, the thermal performance is more susceptible to changes in distance than in angle between tubes. They also reported that the thermal stratification effect of the bottom of the container is lessened and the melting time is shortened with a greater distance. Muneeshwaran et al. [22] examined heat transfer amplification of NC heat sink via notched fin design. Shimoyama et al. [23] analyzed the spontaneous convective HT from heated hollow cylinders arranged in a horizontal disc. They revealed that the conditions of a small space between the horizontal disc and the hollow cylinder and a large space between the hollow cylinders encouraged the reverse flow which can ameliorate the HT rate. Further, oscillatory natural convection of Al₂O₃-water nanofluid in a small horizontal annulus was investigated by Hu et al. [24]. The density inversion of the working fluid may have a substantial efficacy on the temperature and velocity distributions of the NC of Al₂O₃-water nanofluid, according to the results. Nanoparticles can stabilise nanofluid flow and maintain the symmetry of the flow structure. The volume percentage of nanoparticles increases, which improves convective heat transmission. Additionally, a summary of the evolution of the flow regime with the Rayleigh number at various nanoparticle volume fractions is provided. The dynamic viscosity of hydraulic oil HLP 68- Fe₃O₄ – TiO₂ – GO THNF was carried out experimentally by Sepehnia et al. [25] and modelled using machine learning. For mixing ratios of 1:1:1, 1:1:2, 1:2:1, and 2:1:1, respectively, it was discovered the maximum growth in base fluid viscosity in the presence of a 1 % VF of GO : Fe₃O₄ : TiO₂ is 345 %, 1821 %, 1763 %, and 1990 % at a temperature of 15 °C. Additionally, it was discovered that the mixing ratios of 1:1:1, 1:1:2, 1:2:1, and 2:1:1 can lead the viscosity to increase up to 66 %, 75 %, 60 %, and 70 %, respectively, when temperature drops from 65 °C to 15 °C. The works on the related areas are appeared in Refs. [26–28].

Recently, studies based on the second law of thermodynamics have gained popularity to measure the efficiency of thermal systems. The second law examination may be extensive in order to investigate the function of entropy optimization in various thermic systems. THNF natural convection was investigated by Shao et al. [29] in a porous prismatic cage with two moveable hot baffles. They discovered in their research that raising the Frank-Kamenetski number increases streamlines by 6.25 percent, horizontal velocity by 5.086 percent, and vertical velocity by 6.7 percent. They also declared that Bejan number is lessened by 75 % via the augmented Rayleigh number, but 494.14 % more is reinforced considerably by the chamber angle from 45° to 90°. The entropy production for slug flow in a large diameter pipe was investigated by Mohammadi et al. [30]. The ranges of the superficial velocities (SVs) of gas and liquid have been defined at 1.05–3.49 and 0.77–1.2 m/s, respectively. The entropy generation (EG) is extracted using a unique method after the pressure drop, slug length, and frequency being first experimentally tested. Banik et al. [31] examined the entropy analysis of heat transport via thermo magnetic convection in a ferrofluid-filled enclosure. According to a parametric analysis, the configuration using a double-Halbach array produces somewhat better overall results than the one using three regular permanent magnets. Strong advection causes a stronger entropy production at a big field, even if it is seen that the HT increases with raising magnetic field intensity. Among the examined scenarios, an intermediate magnetic Nusselt number is discovered to offer the best cooling.

Using both magnetic configurations, the outcomes were much improved. Other researches in the related fields can be seen in Refs. [32–37].

According to literature survey, many scientists have investigated the natural convection and thermal aspects of nanofluids/hybrid nanofluids in sundry enclosures subject to several constraints of motion. However, the study of natural convection and thermal aspects of ternary hybrid nanofluid inside an inclined domain having a semi-circular heater and triangle-shaped corrugated walls has yet to be investigated. The novelties of this work are.

- Introduction of THNF such as Al_2O_3 +MWCNT + Graphene + water subject to inclined domain.
- Designing of inclined domain with triangle-shaped corrugated walls of variable height.
- Emplacing semi-circular heater on bottom wall of the inclined domain.
- Entropy analysis due to fluid friction and heat transfer subject to inclined domain of complex geometries has been carried out newly.

This study with above novelties (particularly consideration of THNFs) may find significant applications in experimental works of modern industries demanding ultra-model cooling such as car radiators, solar panels, heat exchangers, energy storage devices, heat pipes, heat sinks, and refrigerators. This is feasible due to the very high thermal conductivity of THNF compared to mononanofluid and hybrid nanofluid and accomplishment of prominent heat transfer rate due the presence of triangle-shaped corrugated walls and semi-circular heater.

2. Governing equations

We consider NC of Al_2O_3 +MWCNT + Graphene + water THNF inside an inclined domain which has a semi-circular heater and triangle-shaped corrugated walls as shown in Fig. 1. The inclined domain is featured with a semi-circular heater on the bottom wall. Two inclined walls of the inclined domain are triangle-shaped corrugated walls. The assumptions made for the problem formulation and its solutions are as follows.

- The flow is presumed to be incompressible, Newtonian, laminar, and steady.
- The top and bottom surfaces of the domain except the position of the heater are adiabatic.
- The length (a) of the corrugated walls is constant while their height (b) is variable.
- The nanoparticles such as Al_2O_3 , MWCNT and Graphene, and the water as the base fluid are in thermal equilibrium.
- The heat transportation inside the domain is accompanied by heat generation/absorption.
- The flow is governed by gravity (thermal buoyancy) and domain inclination angle.

Invoking the above information and using Boussinesq theory, the governing equations are ([3,4,6,35,38,39]):

$$\partial_x u + \partial_y v = 0 \quad (1)$$

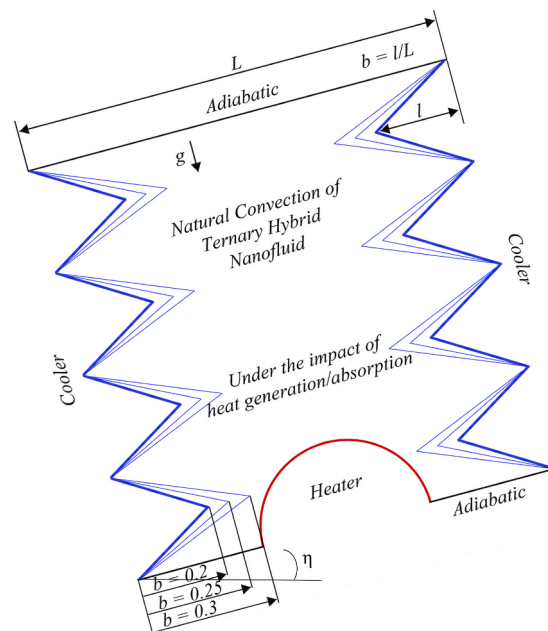


Fig. 1. The geometry examined in this research.

$$u\partial_x u + v\partial_y u = -\frac{1}{\rho_{THNF}}\partial_x p + \frac{\mu_{THNF}}{\rho_{THNF}}(\partial_{xx}u + \partial_{yy}u) + \beta_{THNF}g(T - T_c)\sin(\eta) \tag{2}$$

$$u\partial_x v + v\partial_y v = -\frac{1}{\rho_{THNF}}\partial_y p + \frac{\mu_{THNF}}{\rho_{THNF}}(\partial_{xx}v + \partial_{yy}v) + \beta_{THNF}g(T - T_c)\cos(\eta) \tag{3}$$

$$u\partial_x T + v\partial_y T = \frac{k_{THNF}}{(\rho C_p)_{THNF}}(\partial_{xx}T + \partial_{yy}T) + \frac{1}{(\rho C_p)_{THNF}}Q_0(T - T_c) \tag{4}$$

Here, equation (1) indicates the continuity equation representing the law of conservation of mass, equations (2) and (3) are the momentum equations along horizontal and vertical directions, respectively, representing the law of conservation of momentum, and equation (4) is the energy equation representing the law of conservation of energy. Further, (u,v) are fluid velocities along (x,y) directions, respectively, $\beta_{THNF}, \mu_{THNF}, \rho_{THNF}, (C_p)_{THNF}, k_{THNF}$ are, respectively, thermal expansion coefficient, dynamic viscosity, density, specific heat and thermal conductivity of THNF, Q_0 is the volumetric heat absorption/generation, T is temperature of THNF, and g demonstrates gravitational constant.

The thermo-physical characteristics of THNF are presented in Table 1 as ([2,3]).

where $\rho_{s1}, \rho_{s2}, \rho_{s3}$ are the densities and $\varphi_1, \varphi_2, \varphi_3$ are, respectively, the volume fractions of nanoparticle-1 [Al_2O_3 (spherical)], nanoparticle-2 [MWCNT (cylindrical)], and nanoparticle-3 [Graphene(platelets)], and $\varphi = \varphi_1 + \varphi_2 + \varphi_3$ is the total volume fraction of THNF. Here, ρ_{bf} is the density of base fluid, μ_{bf} is the dynamic viscosity, $(C_p)_{bf}$ is the specific heat, β_{bf} is the thermal expansion coefficient, and k_{bf} is the thermal conductivity of base fluid; $\rho_{s1}(C_p)_{s1}, \rho_{s2}(C_p)_{s2}, \rho_{s3}(C_p)_{s3}$ are specific heat capacity; $\beta_{s1}, \beta_{s2}, \beta_{s3}$ are thermal expansion coefficients, $k_{nf,1}, k_{nf,2}, k_{nf,3}$ are thermal conductivities of nanoparticle-1 [Al_2O_3 (spherical)], nanoparticle-2 [MWCNT (cylindrical)], and nanoparticle-3 [Graphene (platelets)] respectively. Here 1, 2, and 3 stand for Al_2O_3 , MWCNT, and Graphene, respectively.

The thermophysical properties of the base fluid and nanoparticles are mentioned in Table 2.

The tested volumetric fraction of each nanoparticle is given in Table 3.

In order to transform equations (1)–(4) to their non-dimensional forms the following parameters are defined:

Table 1
Thermo-physical characteristics of THNF ([2,3]).

Thermo-physical characteristics	Correlations
Dynamic viscosity	$\mu_{THNF} = (\varphi_1\mu_{nf1} + \varphi_2\mu_{nf2} + \varphi_3\mu_{nf3})/\varphi$ $\mu_{nf1} = (1 + \varphi_1^2 + 2.5\varphi_1)\mu_{bf}$ $\mu_{nf2} = (1 + 904.4\varphi_2^2 + 13.5\varphi_2)\mu_{bf}$ $\mu_{nf3} = (1 + 612.6\varphi_3^2 + 37.1\varphi_3)\mu_{bf}$
Density	$\rho_{THNF} = \varphi_1\rho_{s1} + \varphi_2\rho_{s2} + \varphi_3\rho_{s3} + (1 - \varphi_1 - \varphi_2 - \varphi_3)\rho_{bf}$
Specific heat capacity	$(\rho C_p)_{THNF} = \varphi_1(\rho C_p)_{s1} + \varphi_2(\rho C_p)_{s2} + \varphi_3(\rho C_p)_{s3} + (1 - \varphi_1 - \varphi_2 - \varphi_3)(\rho C_p)_{bf}$
Thermal expansion coefficient	$\beta_{THNF} = \varphi_1\beta_{s1} + \varphi_2\beta_{s2} + \varphi_3\beta_{s3} + (1 - \varphi_1 - \varphi_2 - \varphi_3)\beta_{bf}$
Thermal conductivity	$k_{THNF} = \frac{(\varphi_1 k_{nf1} + \varphi_2 k_{nf2} + \varphi_3 k_{nf3})}{\varphi}$ $k_{nf1} = \left[\frac{2k_{bf} + k_1 + 2(k_1 - k_{bf})\varphi_1}{2k_{bf} + k_1 - (k_1 - k_{bf})\varphi_1} \right] k_{bf}$ $k_{nf2} = \left[\frac{k_2 + 3.9(k_2 - k_{bf})\varphi_2 + k_{bf}}{3.9k_{bf} + k_2 - (k_2 - k_{bf})\varphi_2} \right] k_{bf}$ $k_{nf3} = \left[\frac{k_3 + 4.7(k_3 - k_{bf})\varphi_3 + k_{bf}}{4.7k_{bf} + k_3 - (k_3 - k_{bf})\varphi_3} \right] k_{bf}$

Table 2
Thermophysical properties of water and nanoparticles at 300 K ([2,3,27]).

	ρ (kg m ⁻³)	C_p (J/kg K)	k (W/mK)	β ($\frac{1}{K}$)	μ (Pa.s)	Shape
Water	997.1	4179	0.613	0.00021	0.000857	
Al_2O_3 (nanoparticle 1)	3970	773	40	0.85×10^{-5}	–	Spherical
MWCNT (nanoparticle 2)	2100	3000	740	1.6×10^{-5}	–	Cylindrical
Graphene (nanoparticle 3)	2200	790	5000	-7×10^{-6}	–	Platelets

Table 3
Volumetric fraction of nanoparticles.

Nanoparticles	Volume fraction
Al_2O_3 (nanoparticle 1)	0.01 %
MWCNT (nanoparticle 2)	0.01 %
Graphene(nanoparticle 3)	0.01 %

$$(V, U) = \frac{(v, u)L}{\alpha_f}, P = \frac{\rho L^2}{\rho_f \alpha_f^2}, \theta = \frac{T - T_c}{\Delta T}, (Y, X) = \frac{(y, x)}{L} \quad (6)$$

The non-dimensional governing equations along with their boundary conditions can be obtained as:

$$V\partial_Y U + U\partial_X U = -\left(\frac{\rho_f}{\rho_{THNF}}\right)\partial_X P + \left(\frac{\mu_{THNF}\rho_f}{\rho_{THNF}\mu_f}\right)\text{Pr}(\partial_{XX}U + \partial_{YY}U) + \left(\frac{\rho_{THNF}}{\beta_f}\right)\text{Pr}Ra\theta \sin(\eta) \quad (7)$$

$$U\partial_X V + V\partial_Y V = -\left(\frac{\rho_f}{\rho_{THNF}}\right)\partial_Y P + \left(\frac{\mu_{THNF}\rho_f}{\rho_{THNF}\mu_f}\right)\text{Pr}(\partial_{XX}V + \partial_{YY}V) + \left(\frac{\rho_{THNF}}{\beta_f}\right)\text{Pr}Ra\theta \cos(\eta) \quad (8)$$

$$\left(\frac{k_{THNF}(\rho C_p)_f}{(\rho C_p)_{THNF}k_f}\right)[U\partial_X\theta + V\partial_Y\theta] = \partial_{YY}\theta + \partial_{XX}\theta + Hs\theta \quad (9)$$

$$U = 0, V = 0 \text{ on all surfaces} \quad (10)$$

$$\theta = 0 \text{ on corrugated surfaces}$$

$$\theta = 1 \text{ on heater}$$

$$\partial_y\theta = 0, \text{ on other surfaces}$$

Here, P and p are, respectively, non-dimensional and dimensional pressures. Further, Hs , η , and Ra describe heat generation/absorption parameter, inclination angle, and Rayleigh number, respectively.

Furthermore, the Nusselt number Nu , Entropy generation En , and Bejan number Be could well be specified as:

$$Nu_{loc.} = \left(\frac{k_{THNF}}{k_f}\right)\partial_n\theta|_{on \text{ heater}}, Nu_{ave.} = \frac{1}{S}\int_0^S Nu_{loc.} ds \quad (11)$$

$$En_{Local} = \left(\frac{\mu_{THNF}}{\mu_f}\right)\overbrace{\delta\left[2(\partial_Y V)^2 + 2(\partial_X U)^2 + (\partial_X V + \partial_Y U)^2\right]}^{\text{Entropy due to fluid friction } En_{FF}} + \overbrace{\left(\frac{k_{THNF}}{k_f}\right)\left[(\partial_Y\theta)^2 + (\partial_X\theta)^2\right]}^{\text{Entropy owing to heat transfer } En_{HT}}$$

$$En_{Total} = \int_V En_{Local} dV.$$

$$Be_{loc} = \frac{\left(\frac{k_{THNF}}{k_f}\right)\left[(\partial_Y\theta)^2 + (\partial_X\theta)^2\right]}{En_{Local}}$$

$$Be_{ave} = \frac{\int_A Be_{loc} dA}{\int_A dA}$$

Where S is the heater's length.

3. Numerical approach and validation

In this work, finite element method (FEM) has been applied to solve the governing equations of NC of THNF inside an inclined domain which has a semi-circular heater and triangle-shaped corrugated walls. In this approach, the examined domain is divided into many small, unstructured, and triangle-shaped elements for the purpose of creating nonlinear residual equations for each node within the domain through Galerkin method. These equations can be solved via the Newton-Raphson technique and this process has to be continued until the convergence criterion ($=10^{-5}$) being satisfied. More details of the applied method can be figured out in Refs. [40,41]. In order to check the validity of current outcomes, they have been compared with the numerical and experimental outcomes of Kahveci [42], Khanafer et al. [43], and Krane and Jessee [44] for NC inside a nanofluid-loaded oblique domain and air-filled chamber, respectively, as shown in Fig. 2(a). In addition to this, the results have been checked with numerical findings of Raisi [45] for NC inside a domain heated from below and experimental data of Ho et al. [46] for diverse amounts of volume fraction of nanofluid inside upright square domains as shown in Fig. 2(b) and Table 4. As seen in Fig. 2(a) and (b), and Table 4, a great agreement has been observed.

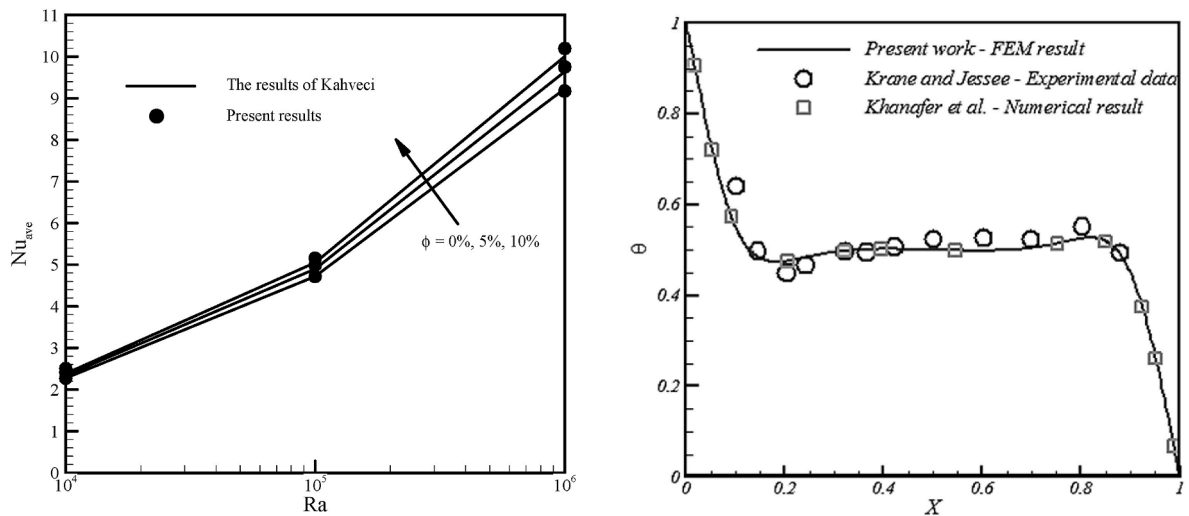


Fig. 2(a). Comparison of the results with numerical and experimental outcomes([42-44]).

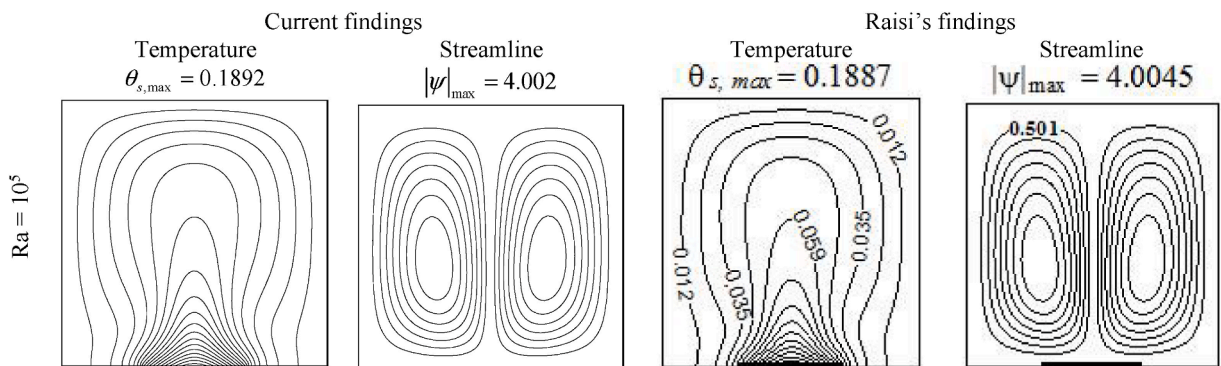


Fig. 2(b). Comparison of the findings with the outcomes of Raisi [45].

Table 4

The current outcomes' validation with experimental data of [46] for Nu_{ave} for diverse amounts of volume fraction of nanofluid.

ϕ (%)	Experimental data of [46]	Current results	Discrepancy (%)
1	32.20	31.91	0.9
2	31.10	30.87	0.74
3	29.08	30.04	3.3

4. Results and discussion

In this part, CFD analysis of natural convection of THNF inside an inclined domain having a semi-circular heater and triangle-shaped corrugated walls is carried out. The non-linear partial differential equations namely energy, momentum, and continuity equations have been solved via FEM. In this discussion, the influence of dimensionless height of the corrugated wall ($b = 0.2, 0.25, 0.3$), Rayleigh number $Ra(10^5, 10^6)$, angle of inclination $\eta(0^\circ, 45^\circ, 90^\circ)$, heat generation/absorption parameter $Hs(-1, 0, 1)$ on streamlines (ψ), isotherms (θ), horizontal velocity (U), vertical velocity (V), entropy generation (En_T), and average Bejan number (Be_{ave}), and local and average Nusselt numbers (Nu_{loc} , Nu_{ave}) have been conveyed with respective suitable profiles.

4.1. Impact of the height of the corrugated wall (b)

Fig. 3 illustrates the influence of the dimensionless height of the corrugated wall ($b = l/L$) on streamlines (ψ), isotherms (θ), horizontal velocity (U), vertical velocity (V), entropy generation (En_T), and Be_{ave} at fixed $Ra = 10^6, \eta = 0^\circ, \phi = 1.5\%$, and $H_s = 1$. At low value of b ($b = 0.2$), two oppositely oriented streamline contours are created in the central region of the domain. Anti-clockwise oriented left-hand side streamline contours are of maximum intensity. On the other hand, clockwise oriented right-hand side streamline contours comprise of minimum value of streamlines. The shape of left and right-hand side streamline contours facing triangular shaped corrugated walls become corrugated. In this case, the THNF adjacent to semi-circular heater gets heated and acquired low density. This heated THNF having low density now moves upward along the cold triangular shaped corrugated walls and then get

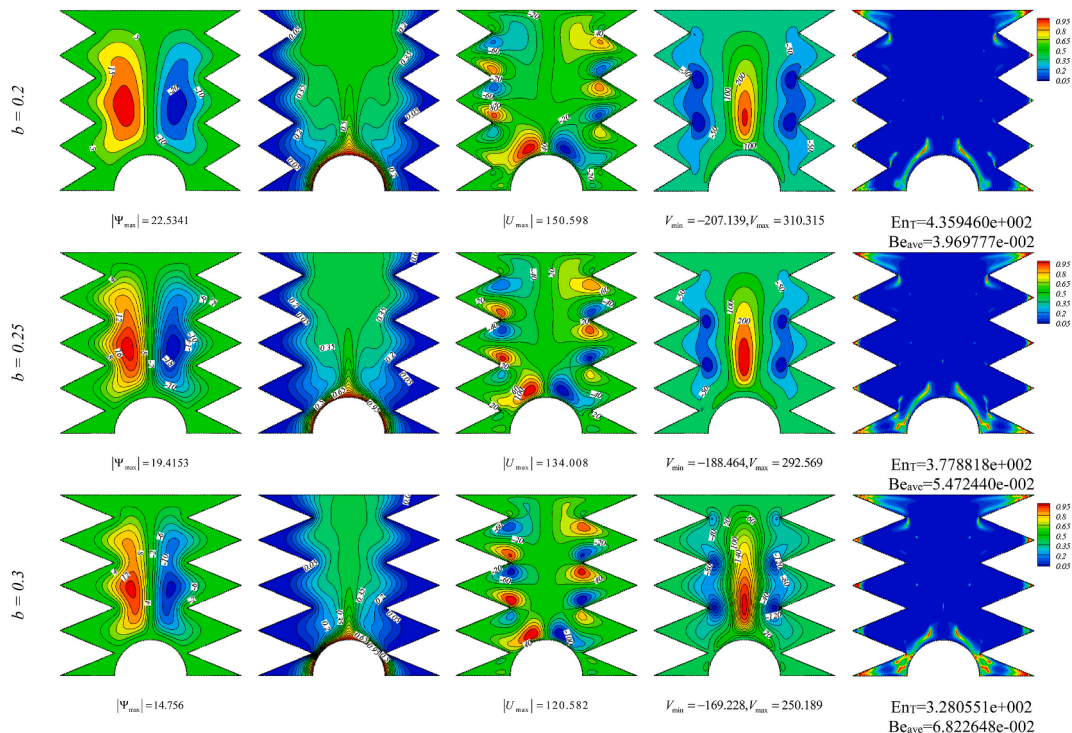


Fig. 3. Influence of height of corrugated walls (b) on streamlines (ψ), isotherms (θ), velocities (U & V), Bejan number (Be_{loc} & Be_{ave}) and entropy generation (Ent) at fixed $Ra = 10^6, \eta = 0^\circ, Hs = 1, \phi = 1.5\%$.

down from the top adiabatic wall of the domain and arrive at the hot semi-circular heater and further rises up. This process leads to the formation of left-hand side anti-clockwise rotated streamline contours. Exactly, in similar process right-hand side streamline contours are developed. The absolute maximum of stream function $|\psi_{\max}|$ is 22.5341. When b increases from 0.2 to 0.25, streamlines whittle down. In this case, the outward facing corrugated shaped and reversely oriented symmetric streamline contours of lower magnitude are created in the central part of the chamber. The absolute maximum stream function $|\psi_{\max}|$ would be 19.4153. The absolute difference of $|\psi_{\max}|$ is 3.1188. The percentage of reduction of $|\psi_{\max}|$ is 13.84%. In fact, a rise in b reduces the temperature gradient between the THNF near the semi-circular heater and corrugated cold wall thereby belittles the convective heat transfer which in turn weakens the streamlines. Moreover, when b increases from 0.25 to 0.3, the streamlines further decrease effectively. The outward facing corrugated shaped streamline contours rotate in opposite directions. As b increases (the height of the corrugated wall enhances), the shape of the corrugation of the streamline contours amplifies. It is in agreement with Selimefendigil et al. [39]. The absolute maximum stream function $|\psi_{\max}|$ is 4.6593. The percentage of reduction of $|\psi_{\max}|$ is $\frac{|\psi_{\max}^{\text{earlier}} - |\psi_{\max}^{\text{present}}|}{|\psi_{\max}^{\text{earlier}}|} \times 100\% = 23.99\%$. In fact, when b increases, the contact surface area between corrugated wall and the THNF enhances. As a result, hot THNF loses significant amount of heat. Therefore, the convective heat transfer becomes less thereby yielding weak streamlines in the domain. It is in consent with Selimefendigil et al. [39]. At any b ($b = 0.2, 0.25, 3.0$), isotherm patterns are featured with centrally created plume shaped temperature line surrounded by less dense wavy shaped vertical temperature lines. This would be because of negligible convective HT of THNF taking place there. However, a good number of dense temperature lines are visualized nearest to the semi-circular heater. This is due to the strong conductive heat transfer from the heater. When b increases a good number of distorted lines in the isotherm pattern are created inside the domain. This can be owing to the strong convective HT of THNF subject to cold corrugated shaped walls of larger height. It is in consent with Selimefendigil et al. [39].

Two big sized horizontal velocity contours of opposite orientations are constructed in the upper part of the domain. The left-hand side upper big sized contour comprises of one maximum horizontal velocity region and two minimum horizontal velocity regions adjacent to the corrugated walls of the domain. In this case, the maximum horizontal velocity region lies between two minimum horizontal velocity regions. Further, right side upper big sized contour contains one minimum horizontal velocity region which lies between two maximum horizontal regions inside the domain. The lower section of the domain contains two reversely oriented big sized horizontal velocity contours. The lower right-hand side contours rotate in clockwise directions while left hand side contours follow opposite direction. The lower left-hand side big contour comprises of maximum horizontal velocity regions and the lower right hand side big contours comprise of minimum horizontal velocity regions only. The horizontal velocity regions of maximum and minimum intensity just lie above the semi-circular heater. Other horizontal velocity regions (maximum/minimum intensity) are formed near the corrugated walls (irrespective of their heights). The absolute maximum of horizontal velocity $|U_{\max}|$ is 150.598. When b raises from 0.2 to 0.25, exactly same horizontal velocity patterns comprising of maximum and minimum horizontal velocity regions are obtained. However, the magnitude of horizontal velocity emaciates. The absolute maximum of horizontal velocity $|U_{\max}|$ is 134.008. The

percentage of reduction of $|U_{max}|$ is 11.02 %. When b further enhances, the upper and lower big sized horizontal velocity contours segregate. However, the maximum and minimum horizontal velocity regions lie adjacent to the corrugated walls of the domain. This segregation would be due to the low convective HT in the presence of corrugated walls of greater height. The absolute maximum of horizontal velocity $|U_{max}|$ is 120.582. The percentage of reduction of $|U_{max}|$ is 10.02 % when b rises from 0.25 to 0.3. The rationale behind this reduction is that a rise in b yields less temperature gradient thereby creating low convective heat transfer. The vertical velocity profiles for different values of b are illustrated. A good number of anti-clockwise rotated vertical velocity contours (enshrining maximum vertical velocity regions) are created in the central part of the domain. This would be owing to the strong convective HT from the semi-circular heater placed at the bottom wall of the domain. However, two other vertical (enshrining minimum vertical velocity regions) of clockwise rotations and wave shape facing the corrugated shaped wall on either side of the domain. The maximum and minimum amounts of vertical velocity are, respectively, $V_{min} = -207.139$ and $V_{max} = 310.315$. When b increases, the structured vertical velocity profiles of decaying magnitude are obtained. In this case, it can be seen that $V_{min} = -188.464$ and $V_{max} = 292.569$. It is visualized that $|V_{min}|$ and $|V_{max}|$ decrease by 9 % and 5.72 %, respectively. When b further increases, heat transfer due to convection in central regions contiguous to the corrugated shaped walls whittle down. In this case, V_{min} and V_{max} would equal to -169.228 and 250.189 , respectively. The percentage decrement of $|V_{min}|$ and $|V_{max}|$ are 10.20 % and 14.48 %, respectively. When b increases, entropy generation En_T decreases effectively. The En_T peters out by 13.32 % and 13.18 % when b increases from 0.2 to 0.25 and 0.25 to 0.3, respectively. The minimum En_T covers the entire domain except the region near the semi-circular heater. The average Bejan number Be_{ave} exhibits opposite trend to that of En_T . It is clear that Be_{ave} enhances by 27 % and 19.79 % when b rises from 0.2 to 0.25 and 0.25 to 0.3, respectively.

4.2. Impact of Rayleigh number (Ra)

Fig. 4 manifests the impact of Ra on streamlines (ψ), isotherms (θ), horizontal velocity (U), vertical velocity (V), entropy generation (En_T), and Be_{ave} at fixed $b = 0.2, \eta = 0^\circ, \phi = 1.5\%$, and $H_s = 1$. At low Raleigh number ($Ra = 10^5$), vertically placed two oppositely oriented symmetric contours of streamlines are visualized. Left-hand side streamline contours of maximum intensity rotate in anti-clockwise direction. These are of corrugated shape facing towards the left corrugated wall of the domain. On the other hand, right-hand side streamline contours of minimum intensity rotate in clockwise direction. These are of corrugated shape facing towards the right corrugated wall of the chamber. The absolute maximum of stream function $|\psi_{max}|$ is 5.03816. When Ra enhances, the streamline contours of greater magnitude are obtained. In fact, amplified Ra accounts for significantly greater convective heat transfer than conductive heat transfer. In other words, greater Ra indicates larger inertial force compared to viscous force. Greater inertial force leads to amelioration of fluid motion of heated THNF near semi-circular heater thereby intensification of convective heat transfer. This is in agreement with Balla et al. [47]. The absolute maximum of $|\psi_{max}|$ is 22.5341 which is significantly higher than the earlier one. The percentage enhancement of $|\psi_{max}|$ is 77.64 % when Ra increases from 10^5 to 10^6 . Weak isotherms are appeared near the cold corrugated walls of the domain. This is because of the fact that HT owing to conduction mechanism would be prominent in the region contiguous to the semi-circular heater. When Ra increases from 10^5 to 10^6 , natural convection heat transfer dominates over the development of thinly populated temperature lines inside the domain. This is in consent with Balla et al. [47]. Highly distorted isotherms indicate the presence of strong convection (augmented thermal conductivity of THNF). In this scenario, thinner thermal boundary layers are envisaged in the region between semi-circular heater and the corrugated walls of the domain. The distorted isotherms are due to the prominent transfer of heat from the bottom wall semi-circular heater to the cold corrugated wall.

The horizontal velocity (U) profiles are featured with four big sized contours (two in upper part and remaining two in lower part of the domain). Each big sized contour comprises of a number of small sized contours representing maximum and minimum horizontal

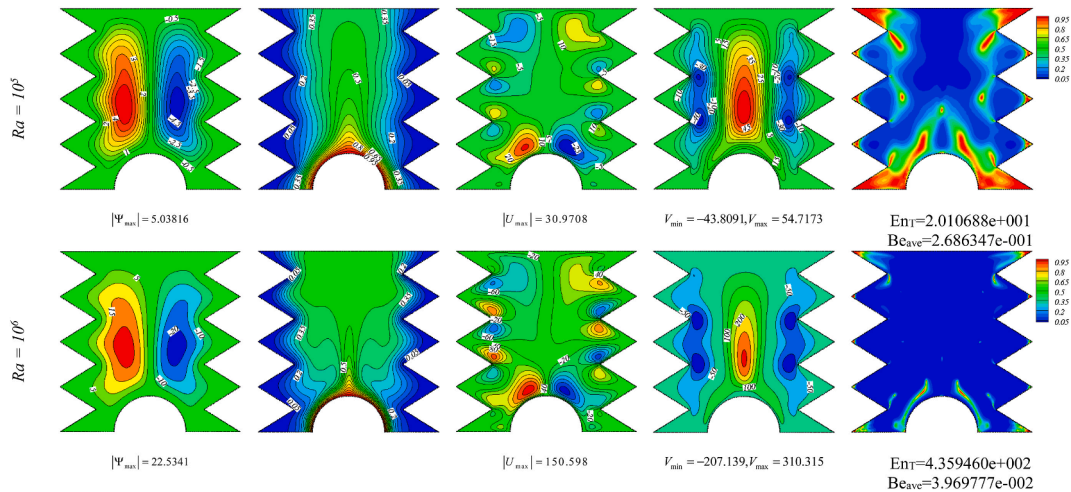


Fig. 4. Influence of Rayleigh number (Ra) on streamlines (ψ), isotherms (θ), velocities ($U&V$), Bejan number ($Be_{loc}&Be_{ave}$) and entropy generation (En_T) at fixed $b = 0.2, \eta = 0^\circ, H_s = 1, \phi = 1.5\%$.

velocities. The absolute maximum of horizontal velocity $|U_{max}|$ is 30.9708. When Ra amplifies, horizontal velocities of same structure and greater strength are obtained. This is because of dominance of buoyancy force caused by greater Raleigh number. When Ra raises from 10^5 to 10^6 , $|U_{max}|$ enhances (from 30.9708 to 150.598) by 79.43 %. At low Ra , the vertical velocity profiles may be featured with anti-clockwise oriented re-circulations in the central part of the domain and clock wise rotated and corrugated shaped re-circulations in the regions near to the corrugated walls of the domain. The centrally created re-circulations indicate vertical velocities of maximum intensity while side-wise created re-circulations represent vertical velocities of maximum velocity. When Ra enhances, the vertical velocities (V_{min} and V_{max}) ameliorate significantly ($|V_{min}|$ rises from 43.8091 to 207.139 and V_{max} grows from 54.7173 to 310.315). This consequence is due to the impact of more buoyancy which is because of the greater Rayleigh number. Percentage increment of $|V_{min}|$ and V_{max} are 372.8 % and 467.12 %, respectively. The entropy generation (En_T) and average Bejan number (Be_{ave}) increase by 116.81 % and 47.78 %, respectively.

4.3. Impact of angle of inclination (η)

Fig. 5 portrays the impact of angle of inclination η on streamlines (ψ), isotherms (θ), horizontal velocity (U), vertical velocity (V), entropy generation (En_T), and average Bejan number (Be_{ave}) at fixed $Ra = 10^6, b = 0.2, \varphi = 1.5\%$, and $H_s = 1$. At horizontal position of the domain ($\eta = 0^\circ$), two re-circulations having corrugated face facing towards the corrugated walls of the domain are formed. Left side corrugated re-circulations representing streamlines of maximum strength rotate in anti-clockwise directions. On the other hand, right side corrugated re-circulations indicating streamlines of minimum strength rotate in clockwise directions. The formation of re-circulations is due to the combination of conduction and convection mechanism. The absolute maximum of stream function $|\psi_{max}|$ is 22.5341. When the domain is inclined at an angle of $45^\circ (\eta = 45^\circ)$, re-circulations of lower strength are obtained. When the angle of inclination η increases, the buoyancy force due to natural convection peters out. Therefore, the convective heat transfer whittles down. This is evidenced by Bondareva et al. [48]. The absolute maximum of stream function $|\psi_{max}|$ is 17.8262. The percentage of diminution is 20.89 %. When $\eta = 90^\circ$, two oppositely oriented streamline contours merge into a bigger contour of streamlines of greater strength. The central part of the domain contains the streamlines of greater strength surrounded by streamlines of lower strength. This is due to strong convective HT than conductive heat transfer. The absolute maximum of stream function $|\psi_{max}|$ is 20.0122. The percentage enhancement is 12.26 %. It is concluded that streamlines reduce its strength within $0^\circ \leq \eta \leq 45^\circ$; however, it reverses its trend lies within $45^\circ \leq \eta \leq 90^\circ$. In fact, an increase in the cavity inclination angle can lead the convective flow to weaken which can result in the reduction of HT rate and fluid flow strength. This is ensured by Bondareva et al. [48].

Isotherms of greater strength appear in the adjacent region of semi-circular heater owing to strong conductive HT while the isotherms of lower strength appear in the region adjacent to the corrugated walls irrespective of the position of the domain (whatever the angle of inclination may be). Further, when η increases from 0° to 45° , isotherms intensify while they decline for a rise in η from 45° to 90° . At $\eta = 0^\circ$, horizontal velocity re-circulations rotating in clockwise directions appear in the top left corner and bottom right corner of the domain. Further, re-circulations of horizontal velocity rotating in anti-clockwise directions appear in the top right corner and bottom left corner of the domain. The re-circulations comprise of the maximum and the minimum horizontal velocity zones. The absolute maximum of horizontal velocity $|U_{max}|$ is 150.598. When η increases from 0° to 45° , a big re-circulation of horizontal velocity rotating in clockwise direction occupies the region from top left corner to the right bottom corner of the domain. Either side of

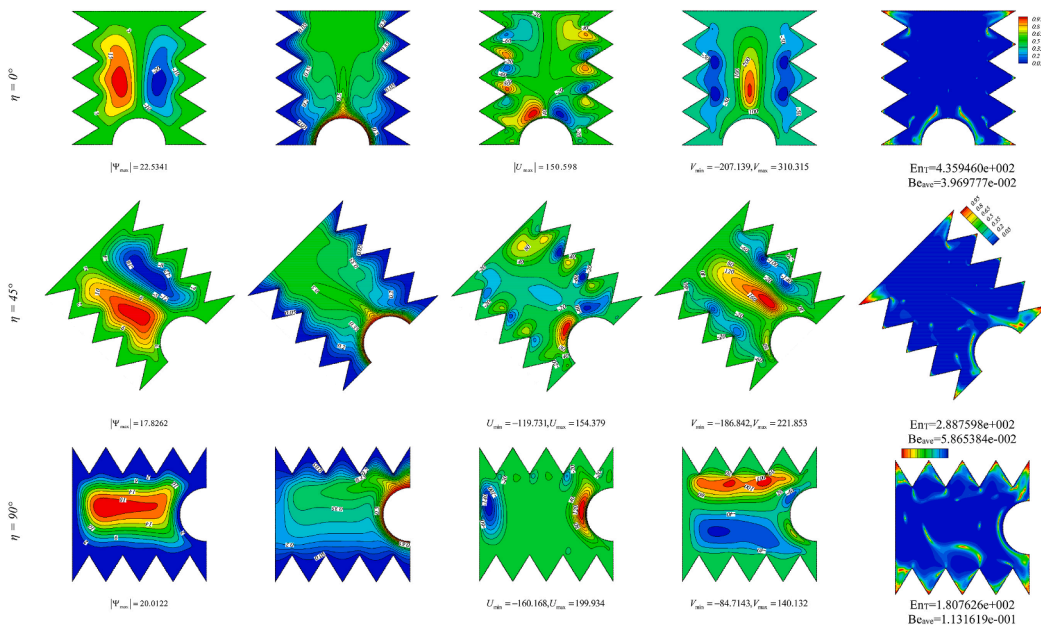


Fig. 5. Influence of cavity inclination angle (η) on streamlines (ψ), isotherms (θ), velocities (U & V), Bejan number (Be_{loc} & Be_{ave}) and entropy generation (En_T) at fixed $Ra = 10^6, b = 0.2, H_s = 1, \varphi = 1.5\%$.

it i.e., top right corner and bottom left corner of the domain accommodate small re-circulations (six in number) orienting in anti-clockwise directions. The strength of horizontal velocity enhances due to domination of convective HT of THNF. The absolute minimum amount of horizontal velocity $|U_{\min}|$ and the maximum amount of horizontal velocity U_{\max} are, respectively, 119.731 and 154.379. The percentage enhancement of U_{\max} is 2.51 % when η increases from 0° to 45° . When η amplifies from 45° to 90° , the entire re-circulation zones merge and then segregate into to bigger re-circulation zones. The re-circulations of horizontal velocity very adjacent to the semi-circular heater rotating in anti-clockwise directions comprise of maximum velocity zones. On the other hand, re-circulations of horizontal velocity very adjacent to the top adiabatic wall rotating in clockwise directions contain minimum velocity zones. In this position of the domain, $|U_{\min}|$ and U_{\max} attain the values 160.168 and 199.934, respectively. The percentage enhancement of $|U_{\min}|$ and U_{\max} are, respectively, 333.77 % and 29.5 % when η increases from 45° to 90° . This is owing to the strong convective HT supported by strong buoyant force. Anti-clockwise rotated re-circulations comprising of maximum vertical velocity zone are developed in the central part of the domain. The lower part of re-circulations looks like semi-circular heater. Clockwise rotated re-circulations having corrugated shape facing the corrugated walls of the cavity and comprising of minimum vertical velocity zones appear either side of the centrally developed re-circulations. The absolute minimum value of vertical velocity $|V_{\min}|$ and the maximum value of vertical velocity V_{\max} are 207.139 and 310.315, respectively. When η increases from 0° to 45° i.e., when the domain is inclined at 45° , the same structured vertical velocity re-circulations are created. At this position of the domain, enhanced buoyant force reduces the vertical velocity (V_{\min} and V_{\max}). The absolute minimum amount of vertical velocity $|V_{\min}|$ and the maximum amount of vertical velocity V_{\max} enhance by 9.8 % and 28.5 %, respectively, when η increases from 0° to 45° . At $\eta = 90^\circ$, anti-clockwise rotated vertical velocity re-circulations comprising of maximum vertical velocity zones appear near the corrugated wall of the domain. Further, clockwise rotated re-circulations comprising of minimum vertical velocity zones are visualized near the bottom corrugated wall of the domain. In addition, two subsidiary vertical velocity zones are created above the semi-circular heater. When η increases from 45° to 90° , enhanced buoyant force favours to the further reduction of vertical velocity. This is observed in Bondareva et al. [48]. The absolute minimum value of vertical velocity $|V_{\min}|$ and maximum amount of vertical velocity V_{\max} enhance by 120.55 % and 96.47 %, respectively. When η increases entropy generation En_T decreases. The En_T reduces by 50.97 % and 37.4 % when η increases from 0° to 45° and 45° to 90° , respectively, while Be_{ave} enhances by 47.7 % for rising η from 0° to 45° and it reduces by 418.32 % when η raises from 45° to 90° .

4.4. Alteration of Nusselt numbers

Fig. 6 illustrates the alteration of Nusselt numbers for different amounts of b, Ra, H_s , and η at fixed values of the remaining useful parameters. The variation of Nu_{local} for diverse amounts of b ($b = 0.2, 0.25, 0.3$) along the length of the heater (S) is shown in Fig. 6(i). It is observed that Nu_{local} decreases with a rise in b near the corrugated walls (at low and high length of the heater) while reverse effect is visualized for the remaining length of the heater. In fact, the temperature gradient is less between the THNF near the initial end/final end of the heater and the peak of the corrugated wall. However, the temperature gradient is more between the THNF at the middle of the heater and the peak of the corrugated wall. It is in consent with Selimefendigil et al. [39]. The minimum amount of Nu_{local} is attained at the mid-point of the heater irrespective the values of b . The absolute difference of Nu_{local} are 0.2563 and 3.0853 when b increases from 0.2 to 0.25 and 0.25 to 0.3. The variation of Nu_{local} for different values of Ra ($Ra = 10^5, 10^6$) is portrayed in Fig. 6(ii). It is seen that Nu_{local} ameliorates with increase in Ra for the entire length of the heater. However, Nu_{local} attains its minimum value at the middle point of the heater. This is due to the fact that a rise in Rayleigh number leads to the strong convective HT from the heater towards the cold corrugated walls of the domain. This is in consent with Balla et al. [47]. The relative enhancement of Nu_{local} is 0.7954 when Ra amplifies from 10^5 to 10^6 . Fig. 6 (iii) manifests the variation of Nu_{local} for sundry heat generation/absorption parameter H_s ($H_s = -1, 0, 1$). It is evident that Nu_{local} is higher when heat absorption ($H_s = -1$) is introduced and it is lower when heat generation ($H_s = 1$) is considered compared to $H_s = 0$ (neither heat absorption nor heat generation). When the heat absorption ($H_s = -1$) is taken into account, the temperature of the THNF within the domain is lessened, that accounts for a larger temperature gradient. This can result in a higher HT rate that indicates a higher Nu . The heat generation, on the other hand, remarkably accounts for the low Nusselt number at low Ra ($Ra = 10^5$). However, at higher Rayleigh number Ra ($Ra = 10^6$), Nusselt number further decreases by heat generation. The rationale behind this phenomenon is that with generating heat the temperature gradient can become smaller which may lead the temperature to become higher. It is very important to mention here that alteration because of heat coefficient is prominent for $Ra \leq 10^5$ where the conduction is the main HT mechanism, while the heat coefficient quickly may lose its impact on Nusselt number for $Ra > 10^5$ due to the fact that the convection motion already dominates the HT at high Ra . It is evident from the observations in Ref. [49]. The variation of Nu_{local} for different values of η ($\eta = 0^\circ, 45^\circ, 90^\circ$) is visualized in Fig. 6 (iv). At horizontal position of the domain, Nu_{local} is minimum at lower and higher length while maximum value of Nu_{local} is obtained at the middle point of the heater. Approximately the same behavior of Nu_{local} is observed for $\eta = 45^\circ$ position of the domain with the exception that minimum value of Nu_{local} is attained a little ahead of the midpoint of the heater. At perpendicular position of the domain ($\eta = 90^\circ$) Nu_{local} has attained the minimum value at initial length of the heater (near the left corrugated wall of the domain) and final length of the heater (near the right corrugated wall of the domain) due to less convective heat transfer. As the length of the heater grows (from left corrugated wall to right corrugated wall of the domain), Nu_{local} gets diminution. It is noticed that Nu_{local} enhances when η grows till the midpoint of the heater from the left corrugated wall while the reverse effect is noticed when η increases from 45° to 90° . The percentage reduction of Nu_{ave} are 10.19 % and 16.75 %, respectively when η increases from 45° to 90° . Indeed, increase in cavity inclination angle leads to an attenuation of convective flow yielding decrease in the HT rate that can be explained by the location of the heater. This is in agreement with Bondareva et al. [48].

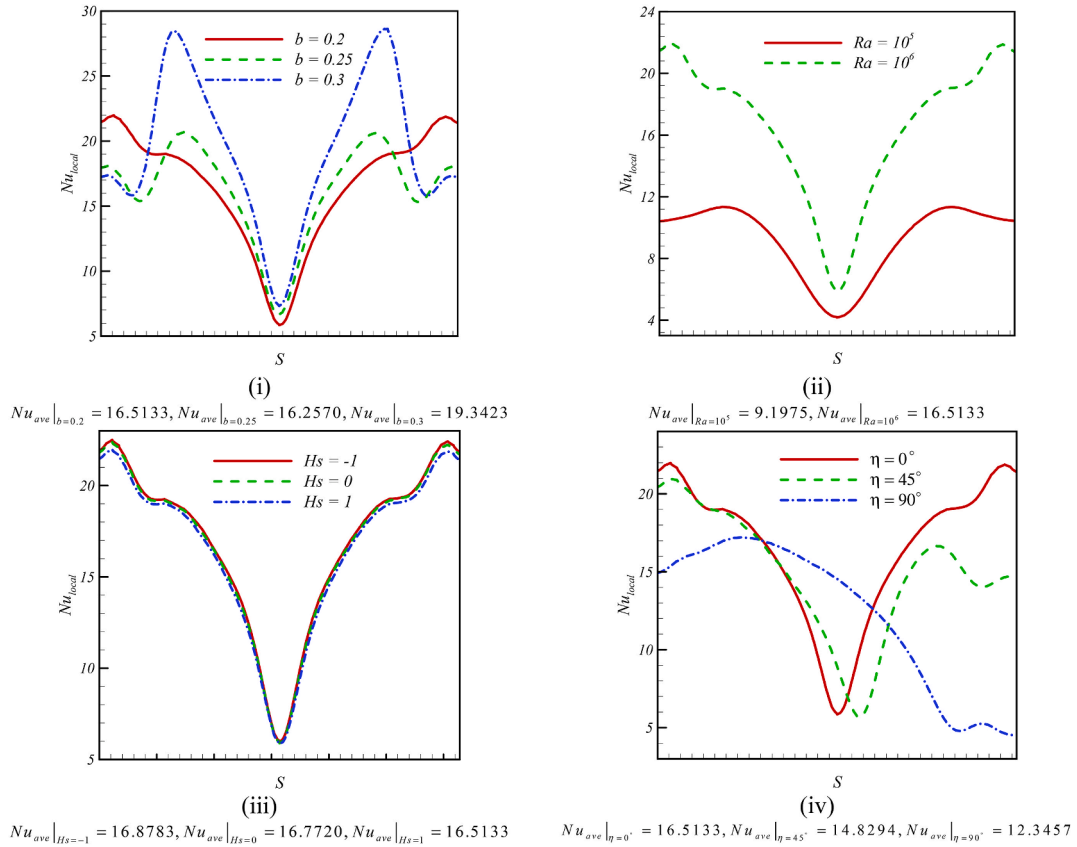


Fig. 6. The influence of height of corrugated walls (b), Rayleigh number (Ra), cavity inclination angle (η), and heat generation/absorption parameter (Hs) on Nusselt numbers.

5. Conclusions

The present work scrutinizes the natural convection and thermal interpretation of THNF through complex geometry such as an inclined cavity with triangle-shaped corrugated walls of variable height and semi-circular heater on its bottom wall. The present problem with complex geometry finds applications in thermal systems involved in geophysical, astrophysical and metallurgical processes. The numerical simulation of the governing equations is carried out by using Finite Element Method. The major outcomes of the present investigation are.

- As dimensionless height of the corrugated wall b increases, streamlines and entropy generation whittle down. Furthermore, a good number of dense temperature lines are visualized nearest to the semi-circular heater. As b enhances, the magnitude of horizontal as well as vertical velocities emaciates by 11.02 % and 14.48 % respectively. In addition, En_T decreases while Be_{ave} exhibits reverse trend to that of En_T with a growth of b . Moreover, Nu_{local} decreases with a rise in b near the corrugated walls (at low and high length of the heater) while reverse effect is visualized for the remaining length of the heater.
- When Ra enhances, the streamlines intensify, the streamlines of greater magnitude are obtained. With an augmentation of Ra , highly distorted isotherms thereby thinner thermal boundary layers are developed. Further, $|U_{max}|$ enhances by 79.43 %, the vertical velocities (V_{min} and V_{max}) ameliorate significantly, Nu_{local} and Nu_{ave} ameliorate with an increase in Ra . Moreover, En_T and Be_{ave} increase by 116.81 % and 47.78 %, respectively, with amplification of Ra .
- When the angle of inclination η increases, streamlines decay down within $0^\circ \leq \eta \leq 45^\circ$, however, it reverses its trend lies within $45^\circ \leq \eta \leq 90^\circ$. The percentage of diminution of $|u_{max}|$ is 20.89 %. Further, when η increases from 0° to 45° and 45° to 90° , isotherms intensify while they decline with a rise in η from 45° to 90° . The $|U_{min}|$ and U_{max} augment by 333.77 % and 29.5 %; $|V_{min}|$ and V_{max} grow by 120.55 % and 96.47 %, respectively, when η ascends from 45° to 90° . As observed, Nu_{local} reduces by 10.19 % and 16.75 %, respectively, when η increases from 0° to 45° and 45° to 90° . It is revealed that Nu_{ave} is prominent at two ends of the heater than at its middle portion with a growth in η . In addition, En_T reduces by 50.97 % and 37.4 % when η increases from 0° to 45° and 45° to 90° , respectively.
- It is visualized that Nu_{local} and Nu_{ave} are maximum subject to heat sink while they attain the minimum values in response to heat source.

The setbacks/limitations of the present work are that the presently expanded industrial world needs ultra-high cooling for the better design and high quality products. However, the present problem may not fulfil that level of expectation. It is very important to maintain the controlled motion within the thermal systems. However, the present problem may not cater to fulfil it up to satisfaction.

In order to fulfil the above gaps the present work may be improved by introducing Darcy-Forchheimer medium so as to enhance the heat transfer rate significantly thereby imparting ultra-high cooling to meet the demands of the ever increasing industrial and manufacturing sectors. Further, the present work may also be improved by considering applied magnetic field so as to better control the fluid motion and double diffusive natural convection facing the situations of both thermal and mass diffusion and modifying the design of the inclined domain with proper placement of cold obstacles within the enclosure so as to ameliorate the heat transfer rate.

Abbreviations

SHC	specific heat capacity
THNF	ternary hybrid nanofluid
TEC	thermal expansion coefficient
TC	thermal conductivity
CNT	carbon nanotube
NC	natural convection
EG	entropy generation
CFD	computational fluid dynamics
FEM	finite element method
MWCNT	multiwall carbon nanotube

Nomenclature

(x,y)	Cartesian coordinates (m)
(u,v)	velocity components along x-and y- directions ($m s^{-1}$)
(X,Y)	non-dimensional Cartesian coordinates (-)
(U,V)	non-dimensional velocities along horizontal and vertical directions (-)
T	fluid temperature in the boundary layer (K)
T_c	temperature of cold corrugated wall (K)
p	pressure (Pa)
η	cavity inclination angle (deg)
g	acceleration due to gravity ($m s^{-2}$)
Q_0	volumetric heat generation/absorption ($J m^{-3} K^{-2}$)
ρ_{THNF}	density of THNF ($kg m^{-3}$)
ρ_{s1}	density of 1st nanoparticle ($kg m^{-3}$)
ρ_{s2}	density of 2nd nanoparticle ($kg m^{-3}$)
ρ_{s3}	density of 3rd nanoparticle ($kg m^{-3}$)
ρ_{bf}	density of base fluid ($kg m^{-3}$)
$(\rho C_p)_{THNF}$	SHC of THNF ($J m^{-3} K^{-1}$)
$(\rho C_p)_{bf}$	SHC of base fluid ($J m^{-3} K^{-1}$)
$(\rho C_p)_{s1}$	SHC of 1st nanoparticle ($J m^{-3} K^{-1}$)
$(\rho C_p)_{s2}$	SHC of 2nd nanoparticle ($J m^{-3} K^{-1}$)
$(\rho C_p)_{s3}$	SHC of 3rd nanoparticle ($J m^{-3} K^{-1}$)
β_{THNF}	TEC of THNF (K^{-1})
β_{s1}	TEC of 1st nanoparticle (K^{-1})
β_{s2}	TEC of 2nd nanoparticle (K^{-1})
β_{s3}	TEC of 3rd nanoparticle (K^{-1})
β_{bf}	TEC of base fluid (K^{-1})
k_{THNF}	TC of THNF ($W m^{-1} K^{-1}$)
$k_{nf,1}$	TC of 1st nanoparticle ($W m^{-1} K^{-1}$)
$k_{nf,2}$	TC of 2nd nanoparticle ($W m^{-1} K^{-1}$)
$k_{nf,3}$	TC of 3rd nanoparticle ($W m^{-1} K^{-1}$)
k_{bf}	TC of base fluid ($W m^{-1} K^{-1}$)
μ_{THNF}	dynamic viscosity of THNF ($Kg s^{-1} m^{-1}$)
μ_{bf}	dynamic viscosity of base fluid ($Kg s^{-1} m^{-1}$)
ϕ_1	volume fraction of 1st nanoparticle (-)
ϕ_2	volume fraction of 2nd nanoparticle (-)
ϕ_3	volume fraction of 3rd nanoparticle (-)
ϕ	total volume fraction of THNF (-)
P	non-dimensional pressure (-)
Ra	Rayleigh number (-)

(continued on next page)

(continued)

H_s	heat generation/absorption parameter (–)
θ	non-dimensional temperature (–)
ψ	dimensional stream function (m^2s^{-1})
Ψ	dimensionless stream function (–)
Nu_{ave}	average Nusselt number (–)
Nu_{loc}	local Nusselt number (–)
En_{total}	entropy generation number (–)
Be_{loc}	local Bejan number (–)
Be_{ave}	average Bejan number (–)
S	heater's length
Subscripts	
ave	average
bf	base fluid
c	cold
loc	local
s	solid particle
THNF	ternary hybrid nanofluid
1	The first nanoparticle
2	The second nanoparticle
3	The third nanoparticle

CRedit authorship contribution statement

M.K. Nayak: Software, Investigation, Formal analysis, Writing, Validation. **M.K. Al Mesfer:** Formal analysis, Methodology, Writing. **A.A. Pasha:** Conceptualization, Writing, Formal analysis. **M. Danish:** Software, Writing. **K. Irshad:** Conceptualization, Simulation, Methodology. **Ali J. Chamkha:** Supervision, Validation.

Declaration of competing interest

The authors declare that they have no known competing financial interests or personal relationships that could have appeared to influence the work reported in this paper.

Data availability

Data will be made available on request.

Acknowledgement

The authors extend their appreciation to the Deanship of Scientific Research at King Khalid University for funding this work through Large groups (project under grant number RGP. 2/512/44).

References

- [1] H. Adun, M. Adedeji, M. Dagbasi, A. Babatunde, Amelioration of thermodynamic performance and environmental analysis of an integrated solar power generation system with storage capacities using optimized ternary hybrid nanofluids, *J. Energy Storage* 51 (2022) 104531.
- [2] S. Kashyap, J. Sarkar, A. Kumar, Performance enhancement of regenerative evaporative cooler by surface alterations and using ternary hybrid nanofluids, *Energy* 225 (2021) 120199.
- [3] R.R. Sahoo, Thermo-hydraulic characteristics of radiator with various shape nanoparticle-based ternary hybrid nanofluid, *Powder Technol.* 370 (2020) 19–28.
- [4] C. Wenhao, L.L. Animasau, Y. Se-Jin, V.A. Oladipupo, J. Xianjun, Simulation of the dynamics of colloidal mixture of water with various nanoparticles at different levels of partial slip: ternary-hybrid nanofluid, *Int. Commun. Heat Mass Tran.* 135 (2022) 106069.
- [5] R. Nasrin Zahan, S. Khatun, Thermal performance of ternary-hybrid nanofluids through a convergent-divergent nozzle using distilled water-ethylene glycol mixtures, *Int. Commun. Heat Mass Tran.* 137 (2022) 106254.
- [6] A. Abbasi, W. Ashraf, Analysis of heat transfer performance for ternary hybrid nanofluid in radiated channel under different physical parameters using GFEM, *J. Taiwan Inst. Chem. Eng.* 146 (2023) 104887.
- [7] Weirong Xiu, L.L. Animasau, Qasem M. Al-Mdallal, Abdullah K. Alzahrani, Taseer Muhammad, Dynamics of ternary-hybrid nanofluids due to dual stretching on wedge surfaces when volume of nanoparticles is small and large: forced convection of water at different temperatures, *Int. Commun. Heat Mass Tran.* 137 (2022) 106241.
- [8] S.K. Rawat, M. Yaseen, M. Pant, C.S. Ujarari, D.K. Joshi, S. Chaube, A.S. Negi, M. Kumar, Designing soft computing algorithms to study heat transfer simulation of ternary hybrid nanofluid flow between parallel plates in a parabolic trough solar collector: case of artificial neural network and particle swarm optimization, *Int. Commun. Heat Mass Tran.* 148 (2023) 107011.
- [9] D. Mohanty, G. Mahanta, S. Shaw, Irreversibility and thermal performance of nonlinear radiative cross-ternary hybrid nanofluid flow about a stretching cylinder with industrial applications, *Powder Technol.* 433 (2024) 119255.
- [10] M.K. Sarangi, D.N. Thatoi, S. Shaw, M. Azam, Ali J. Chamkha, M.K. Nayak, Hydrothermal behavior and irreversibility analysis of Bödewadt flow of radiative and dissipative ternary composite nanomaterial due to a stretched rotating disk, *Mater. Sci. Eng. B* 287 (2023) 116124.
- [11] A. Kumar, M.A. Hassan, Heat transfer in flat tube car radiator with CuO-MgO-TiO₂ ternary hybrid nanofluid, *Powder Technol.* 434 (2024) 119275.
- [12] D.G. Prakasha, M.V.V.N.L. Sudharani, K. Ganesh Kumar, Ali J. Chamkha, Comparative study of hybrid (graphene/magnesium oxide) and ternary hybrid (graphene/zirconium oxide/magnesium oxide) nanomaterials over a moving plate, *Int. Commun. Heat Mass Tran.* 140 (2023) 106557.
- [13] C.S.K. Raju, N. Ameer Ahammad, Kiran Sajjan, Nehad Ali Shah, Se-Jin Yook, M. Dinesh Kumar, Nonlinear movements of axisymmetric ternary hybrid nanofluids in a thermally radiated expanding or contracting permeable Darcy Walls with different shapes and densities: simple linear regression, *Int. Commun. Heat Mass Tran.* 135 (2022) 106110.
- [14] J. Patterson, J. Imberger, Unsteady natural convection in a rectangular cavity, *J. Fluid Mech.* 100 (1) (1980) 65–86.

- [15] V.F. Nicolette, K.T. Yang, J.R. Lloyd, Transient cooling by natural convection in a two-dimensional square enclosure, *Int. J. Heat Mass Tran.* 28 (9) (1985) 1721–1732.
- [16] J.D. Hall, A. Bejan, J.B. Chaddock, Transient natural convection in a rectangular enclosure with one heated side wall, *Int. J. Heat Fluid Flow* 9 (4) (1988) 396–404.
- [17] J.M. Hyun, J.W. Lee, Numerical solutions for transient natural convection in a square cavity with different sidewall temperatures, *Int. J. Heat Fluid Flow* 10 (2) (1989) 146–151.
- [18] Y. Ma, R. Mohebbi, M.M. Rashidi, Z. Yang, Simulation of nanofluid natural convection in a U-shaped cavity equipped by a heating obstacle: effect of cavity's aspect ratio, *J. Taiwan Inst. Chem. Eng.* 93 (2018) 263–276.
- [19] A.M. Zidan, M.K. Nayak, N. Karimi, A.S. Dogonchi, M.K. Chamkha, M.B.B. Hamida, A.M. Galal, Thermal management and natural convection flow of nano encapsulated phase change material (NEPCM)-water suspension in a reverse T-shaped porous cavity enshrining two hot corrugated baffles: a boost to renewable energy storage, *J. Build. Eng.* 53 (2022) 104550.
- [20] M.K. Nayak, N. Karimi, J. Ali, A.J. Chamkha, A. Dogonchi As, S. El-Sapa, A.M. Galal, Efficacy of diverse structures of wavy baffles on heat transfer amplification of double-diffusive natural convection inside a C-shaped enclosure filled with hybrid nanofluid, *Sustain. Energy Technol. Assessments* 52 (2022) 102180.
- [21] J. Wang, Numerical investigation of melting process with natural convection inside multi-tube horizontal cylinder by SPH method, *Int. Commun. Heat Mass Tran.* 145 (2023) 106832.
- [22] M. Muneeshwaran, Ming-Kun Tsai, Chi-Chuan Wang, Heat transfer augmentation of natural convection heat sink through notched fin design, *Int. Commun. Heat Mass Tran.* 142 (2023) 106676.
- [23] R. Shimoyama, Y. Yamada, K. Isobe, A. Horibe, Natural convective heat transfer from a heated horizontal disc with heated hollow cylinders: effect of flow characteristics around heated cylinders with a gap, *Int. Commun. Heat Mass Tran.* 146 (2023) 106928.
- [24] Yu-Peng Hu, Feng-Jun Wang, Yi-Chen Zhang, You-Rong Li, MingHai Li, Oscillatory natural convection of Al₂O₃-water nanofluid near its density maximum in a narrow horizontal annulus, *Int. Commun. Heat Mass Tran.* 136 (2022) 106207.
- [25] M. Sepehria, A. Shahsavari, H. Maleki, A. Moradi, Experimental study on the dynamic viscosity of hydraulic oil HLP 68-Fe₃O₄-TiO₂-GO ternary hybrid nanofluid and modelling utilizing machine learning technique, *J. Taiwan Inst. Chem. Eng.* 145 (2023) 104841.
- [26] M.S. Sadeghi, T. Tayebi, A.S. Dogonchi, M.K. Nayak, M. Waqas, Analysis of thermal behavior of magnetic buoyancy-driven flow in ferrofluid-filled wavy enclosure furnished with two circular cylinders, *Int. Commun. Heat Mass Tran.* 120 (2021) 104951.
- [27] W. Bao, F. Miao, Z. Chao, H. Zhang, W. Zang, C. Dames, C.N. Lau, Controlled ripple texturing of suspended graphene and ultrathin graphite membranes, *Nat. Nanotechnol.* 4 (9) (2009) 562.
- [28] M.K. Nayak, A.S. Dogonchi, A. Rahbari, Free convection of Al₂O₃-water nanofluid inside a hexagonal-shaped enclosure with cold diamond-shaped obstacles and periodic magnetic field, *Case Stud. Therm. Eng.* 50 (2023) 103429.
- [29] Y. Shao, M. K. Nayak, A. S. Dogonchi, Ali J. Chamkha, Y. Elmasry, A. M. Galal, Ternary hybrid nanofluid natural convection within a porous prismatic enclosure with two movable hot baffles: An approach to effective cooling, *Case Stud. Therm. Eng.*, <https://doi.org/10.1016/j.csite.2022.102507>.
- [30] S. Mohammadi, A. Jahangiri, M. Emamzadeh, S. Majidi, A.H.M. Dezfouli, Ali J. Chamkha, Development of the entropy generation investigation for slug flow in a large diameter pipe, *Int. Commun. Heat Mass Tran.* 144 (2023) 106773.
- [31] S. Banik, A.S. Mirja, N. Biswas, R. Ganguly, Entropy analysis during heat dissipation via thermo magnetic convection in a ferrofluid-filled enclosure, *Int. Commun. Heat Mass Tran.* 138 (2022) 106323.
- [32] Wenkai Shao, M.K. Nayak, Rifaqat Ali, S. Nazari, Ali J. Chamkha, Simultaneous numerical examination of thermal and entropy characteristics of Al₂O₃-H₂O nanofluid within a porous diamond shaped container with a L-shaped obstacle, *Case Stud. Therm. Eng.* 54 (2024) 104059.
- [33] K. Irshad, A.A. Pasha, M.K. Al Mesfer, M. Danish, M.K. Nayak, A.J. Chamkha, A.M. Galal, Hydrothermal behavior and entropy analysis of double-diffusive nano-encapsulated phase change materials in a porous wavy H-shaped cavity with baffles: effect of thermal parameters, *J. Energy Storage* 72 (2023) 108250.
- [34] K. Irshad, A.A. Pasha, M.K.A. Mesfer, M. Danish, M.K. Nayak, A.J. Chamkha, A.M. Galal, Second law and thermal analyses of non-Newtonian nanofluid double-diffusive natural convection within a two-hot-baffles-equipped C-shaped domain impacted by magnetic field, *Int. J. Numer. Methods Heat Fluid Flow* 34 (2) (2024) 581–607.
- [35] S.E. Ahmed, Z. Raizah, A.A.M. Arafat, S.A. Hussein, FEM treatments for MHD highly mixed convection flow within partially heated double-lid driven odd-shaped enclosures using ternary composition nanofluids, *Int. Commun. Heat Mass Tran.* 145 (2023) 106854.
- [36] W. Shao, M.K. Nayak, S. El-Sapa, A.J. Chamkha, N.A. Shah, A.M. Galal, Entropy optimization of non-Newtonian nanofluid natural convection in an inclined U-shaped domain with a hot tree-like baffle inside and considering exothermic reaction, *J. Taiwan Inst. Chem. Eng.* (2023) 104990.
- [37] A.A. Pasha, M.K. Nayak, K. Irshad, M.M. Alam, A.S. Dogonchi, A.J. Chamkha, A.M. Galal, Entropy and hydrothermal analyses of nano-encapsulated phase change materials within a U-shaped enclosure: impact of diverse structures of baffles and corrugated wall, *J. Energy Storage* 59 (2023) 106532.
- [38] Sameh E. Ahmeda, Caputo fractional convective flow in an inclined wavy vented cavity filled with a porous medium using Al₂O₃-Cu hybrid nanofluids, *Int. Commun. Heat Mass Tran.* 116 (2020) 104690.
- [39] Fatih Selimefendigil, Hakan F. Oztop, Magnetohydrodynamics forced convection of nanofluid in multi-layered U-shaped vented cavity with a porous region considering wall corrugation Effects, *Int. Commun. Heat Mass Tran.* 113 (2020) 104551.
- [40] Cedric Taylor, Paul Hood, A numerical solution of the Navier-Stokes equations using the finite element technique, *Comput. Fluids* 1 (1) (1973) 73–100.
- [41] T. Basak, S. Roy, T. Paul, I. Pop, Natural convection in a square cavity filled with a porous medium: effects of various thermal boundary conditions, *Int. J. Heat Mass Tran.* 49 (7–8) (2006) 1430–1441.
- [42] K. Kahveci, Buoyancy driven heat transfer of nanofluids in a tilted enclosure, *ASME, J. Heat Tran.* 132 (2010) 062501.
- [43] K. Khanafer, K. Vafai, M. Lightstone, Buoyancy-driven heat transfer enhancement in a two-dimensional enclosure utilizing nanofluids, *Int. J. Heat Mass Tran.* 46 (2003) 3639–3653.
- [44] R.J. Krane, J. Jessee, Some detailed field measurements for a natural convection flow in a vertical square enclosure, *Proceedings of the First ASME-JSME Thermal Engineering Joint Conference* 1 (1983) 323–329.
- [45] A. Raisi, Natural convection of non-Newtonian fluids in a square cavity with a localized heat source, *Journal of Mechanical Engineering/Strojniški Vestnik* 62 (10) (2016).
- [46] C.J. Ho, W.K. Liu, Y.S. Chang, C.C. Lin, Natural convection heat transfer of alumina-water nanofluid in vertical square enclosures: an experimental study, *Int. J. Therm. Sci.* 49 (8) (2010) 1345–1353.
- [47] Shekar Balla Chandra, Naikoti Kishan, Rama S.R. Gorla, B.J. Giresha, MHD boundary layer flow and heat transfer in an inclined porous square cavity filled with nanofluids, *Ain Shams Eng. J.* 8 (2017) 237–254.
- [48] Nadezhda S. Bondareva, Mikhail A. Sheremet, Hakan F. Oztop, Nidal Abu-Hamdeh, Heatline visualization of MHD natural convection in an inclined wavy open porous cavity filled with a nanofluid with a local heater, *Int. J. Heat Mass Tran.* 99 (2016) 872–881.
- [49] A. Abdulkadhim, H.K. Hamzah, F.H. Ali, Çağatay Yıldız, A.M. Abed, E.M. Abed, M. Arıcı, Effect of heat generation and heat absorption on natural convection of Cu-water nanofluid in a wavy enclosure under magnetic field, *Int. Commun. Heat Mass Tran.* 120 (2021) 105024.